RSC Advances

ROYAL SOCIETY OF CHEMISTRY

www.rsc.org/advances

Journal Name

ARTICLE

Non-covalent Functionalization of Graphene Oxide by Pyrene-Block Copolymers for Enhancing Physical Properties of Poly (methyl methacrylate)

Received 00th January 20xx,
Accepted 00th January 20xx

DOI: 10.1039/x0xx00000x

www.rsc.org/

Shiqiang Song,[a] Chaoying Wan,*[b] Yong Zhang*[a]

Pyrene-functionalized poly (methyl methacrylate)-block-polydimethylsiloxane (Py-PMMA-*b*-PDMS) copolymers were synthesized via activators regenerated by an electron transfer atom transfer radical polymerization (ARGET ATRP) method and further used to functionalize graphene oxide (GO) through the π-π interaction between pyrene and the carbon sheets. The modification efficiency of the non-covalently functionalized GO (GO@Py-PMMA-*b*-PDMS) particles was evaluated by studying their effects on the mechanical, optical and thermal properties of the PMMA. With incorporation of 0.05 wt% GO@Py-PMMA-*b*-PDMS, the tensile strength, Young's modulus, elongation at break and toughness of PMMA were increased by 23%, 54%, 117%, and 218%, respectively, showing simultaneously reinforcing and toughening effects of the functionalized GO particles; the initial decomposition temperature of PMMA increased by 11 °C from 349 °C to 360 °C; and the haze value of PMMA increased from 2.1% to 16.8%; the refractive index of PMMA varied from 1.48 to 1.51. This improvement in the physical properties of PMMA can be attributed to the homogeneous dispersion and enhanced interfacial adhesion between GO@Py-PMMA-b-PDMS and PMMA. This work demonstrates the feasibility of using GO@Py-PMMA-b-PDMS as a modifier for simultaneously improving the mechanical, optical and thermal properties of PMMA for potential organic light-emitting diodes and organic photovoltaics applications.

1. Introduction

Graphene oxide (GO) has attracted great attention in material modification because of its extraordinary properties such as good mechanical, barrier and electrical properties.[1-3] Its abundant surface functional groups and high aspect ratio make it particularly preferable for reinforcement of polymers,[4-6] and the reinforcement efficiency depends on its dispersion and interfacial interactions with polymers. Various methods have been under developing in order to facilitate the dispersion of GO in polymers, such as directly physical-distribution with the assistance of ultrasonication[7-9] and high shear mixing,[10-11] or chemical functionalization of the GO surface to improve the compatibility with polymers. The chemical functionalization of GO including covalent[12-14] and non-covalent[15-16] bonding can further enhance the interfacial interactions between GO with various polymers, and benefit the reinforcement efficiency. However, covalent bonding may inevitably disrupt the extended π-π conjugation in GO carbon sheets, combined with the conversion of sp^2 carbons to sp^3 by hybridization[17]. For example, a strong coupling between graphene based fillers and polymer chains may lead to damping of phonon or scattering at the boundaries, reducing phonon speed or mean free path, thus limiting the intrinsic thermal conductivity of the fillers. In comparison, non-covalent bonding through H-π, π-π, cation-π, anion-π, and nonpolar gas-π interactions can well preserve the intrinsic conductivity of graphene sheets, as well as facilitate the dispersion of graphene/GO sheets in polymers.

The π-π interactions are one of the most intriguing non-covalent interactions in the sense that the negatively charged and diffuse electron clouds of the π systems exhibit an attractive interaction between graphene nanosheets and organic molecules,[18-22] e.g., the

[a] *School of Chemistry and Chemical Engineering, State Key Laboratory for Metal Matrix Composite Materials, Shanghai Jiao Tong University, Shanghai 200240, People's Republic of China.*
E-mail: yong_zhang@sjtu.edu.cn (Y. Zhang)
[b] *International Institute for Nanocomposites Manufacturing, WMG, University of Warwick, CV4 7AL, UK.*
E-mail: Chaoying.Wan@warwick.ac.uk (C. Wan.).
†Electronic Supplementary Information (ESI) available: GPC of Py-PMMA-Br and Py-PMMA-*b*-PDMS, FTIR spectra of GO, GO@Py-PMMA-*b*-PDMS and Py-PMMA-*b*-PDMS, DSC spectra, SEM images and summary of composites mechanical properties. See DOI: 10.1039/x0xx00000x

pyrene moiety has a strong affinity toward the basal plane of graphite via π-π stacking.[18] Water-soluble pyrene derivative 1-pyrenebutyrate[15] and pyrene butanoic acid succidymidyl ester (PBSA)[19] were reported for stabilizing graphene sheets. The π-π interactions between graphene and PBSA have a negligible effect on the optical adsorption of the graphene film in the visible light region. Apart from pyrene functionalization, GO can also be non-covalently functionalized by conjugated and aromatic polymers such as polyaniline and polystyrene (PS). Graphene nanosheets were non-covalently modified with sulfonated polyaniline leading to a water-soluble composite.[20] PS modified graphene nanosheets via a one-step method, resulting in electrically conductive graphene/PS nanocomposites with homogeneous graphene dispersion.[20] Therefore, the non-covalent method utilizing π-π interactions of graphene sheets provides a facile and nondestructive method for graphene and GO modification.

In this article, a block copolymer composed of poly (methyl methacrylate) (PMMA) and polydimethylsiloxane (PDMS) backbone terminated with pyrene moiety was synthesized. The pyrene moiety was used to interact with GO via π-π stacking in order to create the PMMA-*b*-PDMS block copolymer grafted GO particles to facilitate the dispersion in PMMA matrix. The effects of such Py-PMMA-*b*-PDMS functionalized GO on the mechanical, thermal and optical properties of PMMA were discussed.

2. Experimental

2.1. Materials and characterization.

Flake graphite (99.8%) with average particle size of 45 um was purchased from Alfa Aesar (China) Chemical Co., Ltd. Graphene oxide (GO) was prepared according to a previous procedure reported by our laboratory.[23] PMMA (PLEXIGLAS® Resist zk50) was made by Evonik Co. Methyl methacrylate (MMA, 98%) was passed through a basic alumina column and distilled prior to use. Vinyl terminated polydimethylsiloxane (VTPDMS) was used as received from Jiangxi Xinghuo Chemical Co., Ltd., China. All the other chemicals were used as received unless otherwise noted.

FTIR spectra were obtained on a Perkin-Elmer Paragon 1000PC spectrometer as the background from 400-4000 cm^{-1}. UV-Vis absorption spectra were recorded with a UV-2550 spectrophotometer (Shimadzu, Japan). The emission spectra were recorded on a Perkin-Elmer LS 50B luminescence spectrometer at room temperature. The chemical state of the surface was characterized by X-Ray photoelectron spectroscopy (XPS) on an RBD upgraded PHI-5000C ESCA system (Perkin-Elmer) with Al K_a radiation (hv=1486.6 eV). M_n, M_w and PDI (M_w/M_n) of the polymers were measured with GPC (HLC-8320GPC, TOSOH, Japan), with PMMA as a reference standard and DMF as an eluent. ^{1}H-NMR (400 MHz) spectra were measured using a Bruker spectrometer in $CDCl_3$ at ambient temperature. Thermal stabilities were measured via thermogravimetric analysis in nitrogen with a TA Instruments model Q2000 at a heating rate of 20 ˚C/min. DSC was used to measure glass transition temperature (T_g) using a TA Q2000 instrument in nitrogen atmosphere at the heating rate of 20 °C/min from -80 to 150 °C and a cooling rate of 10 °C/min. The tensile properties of composites were measured with an Instron 4465 tensile machine at 30 °C with a humidity of about 25% at a crosshead speed of 2 mm/min for PMMA and its composites with the initial gauge length of 20 mm. The samples were cut into strips of 30×4 mm^2 with a razor blade and five strips were measured for each sample. Atomic force microscopic (AFM) analysis of the surface of GO@Py-PMMA-*b*-PDMS was conducted on a Nanoscope IIIa scanning probe microscope (Digital Instruments, Santa Barbara, CA) mounted with silicon tips (125 μm in length and 500 kHz resonant frequency) in tapping mode under ambient conditions, and the scan rate was 2.0 Hz. The morphology of GO@Py-PMMA-*b*-PDMS was observed by transmission electron microscopy (TEM) (JEOL2100F). The dispersion of GO@Py-PMMA-*b*-PDMS was obtained by ultrasound treatment in DMF (0.01mg/ml) for 30 min. Samples were prepared by dropping the dispersion onto mica films and the copper grid, respectively, and dried at room temperature overnight for AFM and TEM analysis. Refractive index was measured by a variable angle spectroscopy ellipsometry (VASE) (JA Woollam Co.,Inc.), and data were taken at 632.8 nm.

2.2. Synthesis of 1-pyrenylmethyl 2-bromopropanoate ARGET-ATRP initiator (Py-Br)

An initiator was synthesized from 1-pyrenemethanol and 2-bromo-2-methylpropionyl bromide according to the literature.[24] Briefly, 1-pyrenemethanol (1 g, 4.31 mmol) and triethylamine (0.46 g, 6.46 mmol) were dissolved in dry THF (10 mL) in a 50 ml three-necked flask which was flamed and dried under vacuum. Then 2-bromo-2-methylpropionyl bromide (1.17 g, 5.17 mmol) was dissolved in dry THF (10 mL) and added to the above solution dropwise at 0°C over a period of 10 min. After stirring for 4 h at room temperature, the reaction system was filtered, concentrated, re-dissolved in dichloromethane and extracted three times with a K_2CO_3 aqueous solution. The organic phase was separated, dried over magnesium sulfate, filtered, and evaporated to dryness. 1-pyrenylmethyl 2-

bromopropanoate (Py-Br) was obtained after recrystallization in methanol and vacuum drying (yield: 91%).

2.3. Synthesis of Pyrene-labeled poly (methyl methacrylate) ARGET-ATRP macroinitiator (Py-PMMA-Br).

In a typical experiment, 1-pyrenylmethyl 2-bromopropanoate (Py-Br) (25.5 mg, 0.067 mmol) was injected into a 25 ml round-bottomed flask containing DMF (2.7 g), MMA (2.7 g, 28.6 mmol), PMDETA (11.5 mg, 0.067 mmol), $CuBr_2$ (1.5 mg, 6.7 μmol), and Tin_2-ethylhexanoate [$Sn(EH)_2$] (22.0 μL, 0.067 mmol) under nitrogen atmosphere. The flask was sealed with a rubber septum and purged with nitrogen for 5 min in an ice-bath, before being placed in an oil bath at 60 ˚C. After polymerization for 8 h, the mixture was exposed to air and diluted in CH_2Cl_2, and then the solution was passed through a basic alumina column. After being condensed, the polymer was precipitated twice from excess amounts of cold methanol, filtered, and dried under vacuum for 24 h. The yield was equivalent to 54% conversion of the monomer.

2.4. Synthesis of poly (methyl methacrylate)-*block*-polydimethylsiloxane, (Py-PMMA-*b*-PDMS) by ARGET-ATRP.

Py-PMMA-Br macroinitiator ($M_{n,GPC}$ = 2.70×10^4 g/mol and PDI=1.45) (0.27 g, 0.01 mmol) was dissolved in DMF (10 mL) in a dried 50 ml round-bottomed flask and bubbled with nitrogen for 15 min. VTPDMS ($M_{n,GPC}$ =5.37×10^3 g/mol and PDI=1.12) (2.15 g, 0.4 mmol) dissolved in THF (10 ml) was transferred to the flask via a syringe. Next a solution of PMDETA (0.34 mg, 0.002 mmol) /$CuBr_2$ (0.44 mg, 0.002 mmol) complex in degassed DMF (0.1 mL) was added. The resulting mixture was stirred for 10 min before a purged solution of $Sn(EH)_2$ (0.18 mg, 0.001 mmol) in DMF (0.1 mL) was added. The sealed flask was purged with nitrogen for 15 min before placed in thermostated oil bath at 60˚C. The polymerization was stopped after 48 h ($M_{n,GPC}$=4.59×10^4 g/mol, PDI=1.74 conversion=8.7%) by opening the flask and exposing to air. The polymer was precipitated twice from excess amounts of cold methanol, filtered, and dried under vacuum for 24 h.

2.5. Preparation of GO@Py-PMMA-*b*-PDMS/PMMA composite.

GO@Py-PMMA-*b*-PDMS/PMMA composites with different GO contents were prepared by solution blending. A typical procedure of preparing GO@Py-PMMA-*b*-PDMS/PMMA composites containing 0.5 wt% GO was as follows: a suspension consisting of GO (10 mg) and Py-PMMA-*b*-PDMS (10 mg) in 50 ml DMF was sonicated for 1 h, and stirred at room temperature for 24 h. The resultant product was separated by centrifugation at 10,000 rpm followed with DMF-washing steps to remove the physically adsorbed or free polymers. Finally, the GO@Py-PMMA-*b*-PDMS was mixed with a solution containing 2 g PMMA in 50ml DMF and sonicated for 30 min, and precipitated in excess methanol, filtered, washed and dried in vacuum at 60˚C for 4 day to obtain a GO@Py-PMMA-*b*-PDMS/PMMA composite. The other composites containing 0.05, 0.2, 0.5, and 1 wt% of GO were prepared with the same procedure. Composites films were compression-molded into plates with a thickness of 130 um (10×10 cm^2) on an LP-S-50 molds (LabTech Engineering Company Ltd) at 190 °C for 15 min and at room temperature for 10 min.

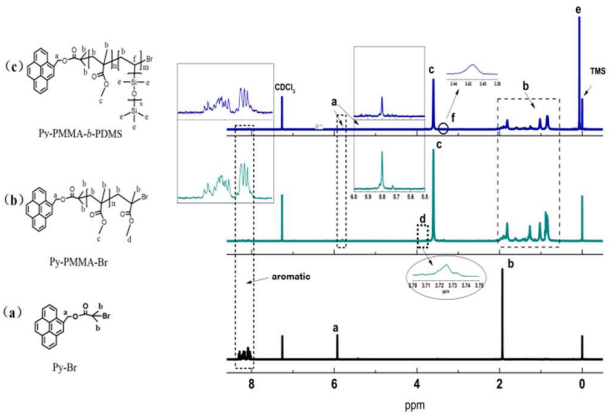

Fig. 1 ^{1}H-NMR spectra of (a) Py-Br, (b) macroinitiator Py-PMMA-Br and (c) Py-PMMA-*b*-PDMS.

3. Results and discussion

3.1 Characterization of Py-PMMA-Br and Py-PMMA-*b*-PDMS.

Py-PMMA-Br was prepared by activators regenerated by ARGET ATRP using Py-Br initiator, $CuBr_2$/$Sn(EH)_2$ catalyst and PMDETA ligand. Py-PMMA-*b*-PDMS was also prepared by ARGET-ATRP in the presence of VTPDMS and Py-PMMA-Br as macromolecular initiator (Scheme 1A). The structure of Py-Br, Py-PMMA-Br and Py-PMMA-*b*-PDMS was characterized by ^{1}H-NMR (Fig. 1), and the positions of the marked protons of Py-Br were shown by the corresponding peaks in the ^{1}H-NMR spectrum (Fig.1a). In Fig.1b, the chemical shift at 3.75 ppm (d in Fig.1b) was attributed to the methyl ester group at the chain end of Py-PMMA-Br, which was deviated from the chemical shift (3.60 ppm, c in Fig.1b) of the other methyl ester groups of PMMA component in Py-PMMA-Br, because of the electron-withdrawing effect of ω-Br atom.[25] In the NMR spectra of Py-PMMA-Br (Fig.1b), two new peaks ‘c and d’ appeared, indicating the polymerization of Py-Br and MMA. In

Fig.1c, apart from the peaks of Py-PMMA-Br (a, b, c, d), Py-PMMA-*b*-PDMS showed a new peak at ca. 0.1 ppm (-Si-CH_3) (e), demonstrating VTPDMS was copolymerized with Py-PMMA-Br by ARGET-ATRP. It is worth noting that in Fig.1a~c, the peaks intensity of pyrene ring became increasingly weaker with the PMMA and PDMS segment content increasing. M_n and PDI of Py-PMMA-Br and Py-PMMA-*b*-PDMS copolymer were measured by GPC with PMMA as a reference standard and DMF as an eluent (Table S1 and Fig.S1 in the Supporting Information). It can be concluded that a block copolymer Py-PMMA-*b*-PDMS has been successfully synthesized by ARGET-ATRP.

3.2 Characterization of GO@Py-PMMA-*b*-PDMS.

GO@Py-PMMA-*b*-PDMS was prepared by a non-covalent (π-π stacking) modification method and the preparation steps were presented in Scheme 1B. Pyrene groups in Py-PMMA-*b*-PDMS can interact with the graphitic surfaces of GO through effective π-π stacking interaction, leading to strongly attachment between Py-PMMA-*b*-PDMS and GO surfaces. In Scheme 1[B(a)], it also can be seen that GO was fully exfoliated in DMF after slight sonication for 1h, formed a stable and homogeneous GO dispersion. Py-PMMA-*b*-PDMS was added into the GO dispersion to obtain a stable and homogeneous mixture dispersion (Scheme 1[B(b)]). There were no precipitates in the two dispersions in 24 h after stopping stirring.

(A) Synthesis of Py-PMMA-*b*-PDMS (block copolymer) by ARGET-ATRP.

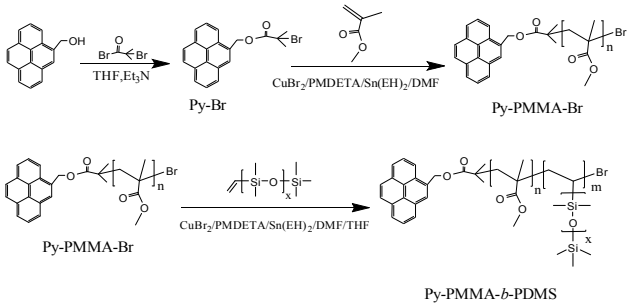

(B) Preparation of GO@Py-PMMA-*b*-PDMS/PMMA composite.

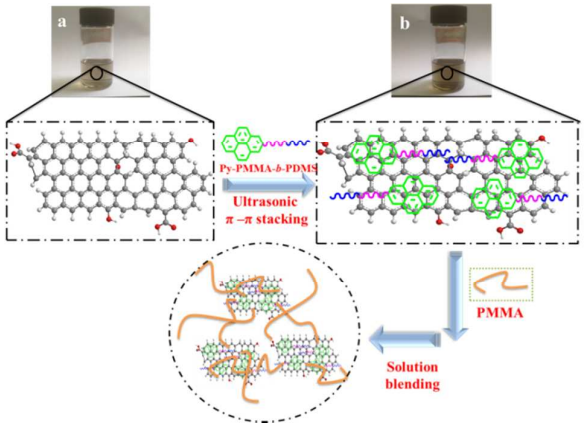

Scheme 1 Schematic illustration for (A) Synthesis of Py-PMMA-*b*-PDMS (block copolymer) by ARGET-ATRP and (B) preparation of GO@ Py-PMMA-*b*-PDMS and its PMMA composites

FTIR spectra were used to probe the introduction of Py-PMMA-*b*-PDMS into the structure of GO@ Py-PMMA-*b*-PDMS. In Fig.S2 (in the Supporting Information), GO spectrum revealed vibration bands corresponding to C=O stretching at 1734 cm^{-1}, C=C stretching at 1589 cm^{-1} and the asymmetric stretching C-O-C at 1150 and 1045 cm^{-1} (Fig. S2a).[26] Py-PMMA-*b*-PDMS spectrum shows stretching vibration of C=O group at 1734 cm^{-1} typical of the carboxyl group of PMMA, asymmetric stretching vibration of Si-O-Si at 1000-1200 cm^{-1} (Fig. S2c). The presence of the above mentioned peaks in GO@Py-PMMA-*b*-PDMS (Fig.S2b) indicates the successful functionalization of GO with Py-PMMA-*b*-PDMS.

XPS analysis was performed to probe the compositions of Py-PMMA-*b*-PDMS and GO@ Py-PMMA-*b*-PDMS. In Fig.2a, there were C, O and Si elements in Py-PMMA-*b*-PDMS and GO@Py-PMMA-*b*-PDMS, indicating that Py-PMMA-*b*-PDMS was successfully synthesized by ARGET-ATRP and introduced into GO, respectively. The spectra of the C_{1s} electron orbital (Fig.2b-c) indicated the existence of five carbon components: C_{sp2} / C_{sp3} (284.8 eV), C-O bond (285.6 eV), C=O bond (286.7 eV), O=C-O bond (289.0 eV) and C-Si bond (284.4 eV).[27] The existence of C-Si bonds also demonstrated the successful synthesis of Py-PMMA-*b*-PDMS (Fig.2b) and introduction of Py-PMMA-*b*-PDMS into the GO@ Py-PMMA-*b*-PDMS (Fig.2c), which was in good agreement with the result of FT-IR.

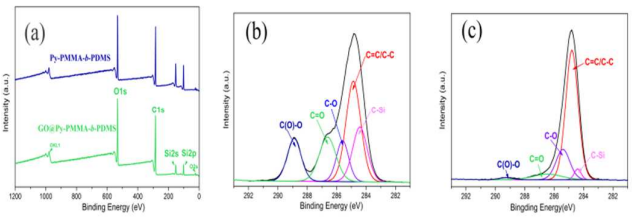

Fig.2 XPS spectra of Py-PMMA-*b*-PDMS and GO@ Py-PMMA-*b*-PDMS (a); high resolution scans of C_{1s} region of Py-PMMA-*b*-PDMS (b) and GO@ Py-PMMA-*b*-PDMS (c).

UV-Vis absorption spectra indicated the introduction of Py-PMMA-*b*-PDMS into surface of GO by π-π stacking. In the spectra (Fig. 3a), Py-PMMA-*b*-PDMS solution in DMF has two peaks at 328 and 344 nm, due to π-π* transitions of aromatic C-C bonds of pyrene.[28] The two peaks of pyrene became very weak in intensity and exhibited a small blue shift (3 nm) in GO@ Py-PMMA-*b*-PDMS solution in DMF, which should be ascribed to π-π stacking between the pyrene groups in Py-PMMA-*b*-PDMS and GO. This change in the peaks implies the successful π-π stacking and strong interaction between Py-PMMA-*b*-PDMS and GO.[15, 28, 29] Photoluminescence (PL) spectra were used to further confirm the π-π stacking. The Py-PMMA-*b*-PDMS solution (Fig. 3b) showed emission peaks at 276 and 396 nm on irradiation at 343 nm, while the GO@ Py-PMMA-*b*-PDMS solution showed emission peaks at 273 and 393 nm with relatively slightly lower peak intensity. These changes in the position and intensity can be explained by that GO acted as a superquencher and arose from an efficient energy transfer of excitons through π-π interaction.[30] The results were consistent with UV-Vis absorption. It can be concluded that π-π stacking should be present between Py-PMMA-*b*-PDMS and GO, resulting in Py-PMMA-*b*-PDMS adsorbed onto GO.

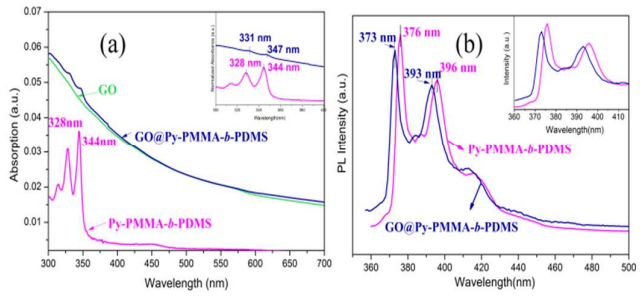

Fig.3 (a) UV-Vis spectra of GO, Py-PMMA-*b*-PDMS and GO@ Py-PMMA-*b*-PDMS solutions in DMF at a concentration of 0.05mg/ml (inset: the absorption at 300-400 nm) and (a) photoluminescence spectra of Py-PMMA-*b*-PDMS and GO@ Py-PMMA-*b*-PDMS solutions in DMF at a concentration of 0.05mg/ml on irradiation at 343 nm (inset: the PL at 360-420 nm).

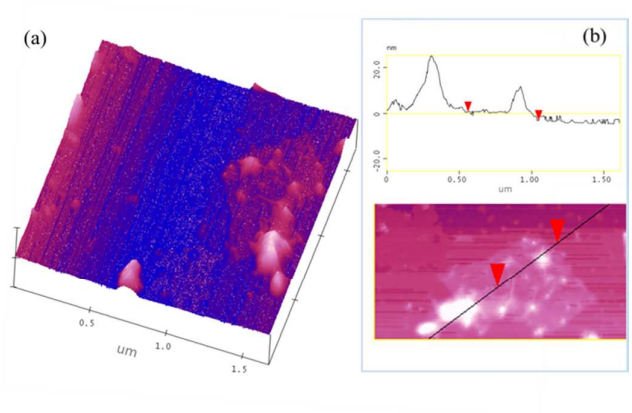

Fig.4 AFM photograph (a) and height profile (b) of GO@Py-PMMA-*b*-PDMS

Furthermore, to get direct evidence of the absorption of Py-PMMA-*b*-PDMS on the GO, the AFM image illustrated a representative height of GO@Py-PMMA-*b*-PDMS deposited on Si substrate as shown in Fig.4. It can be clearly seen that Py-PMMA-*b*-PDMS adsorbed onto GO with the maximum height ca. 25 nm. The absorption of Py-PMMA-*b*-PDMS on the GO was also proved by TEM images. In Fig.5a, Py-PMMA-*b*-PDMS macromolecules were well absorbed on GO surfaces with good dispersion. As expected, when the Py-PMMA-*b*-PDMS was introduced into the GO by π-π stacking, the TEM images (Fi.5b) clearly presented that the Py-PMMA-*b*-PDMS macromolecules were attached and absorbed on the surface of GO surfaces due to the π-π stacking as evidenced from the UV-Vis and PL spectra. This results directly indicates the successful introduction of Py-PMMA-*b*-PDMS into GO.

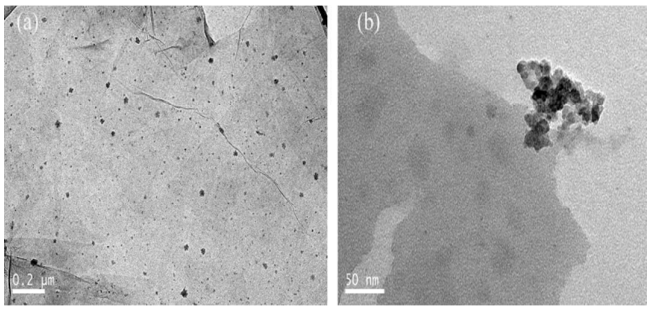

Fig.5 TEM images of (a) GO@Py-PMMA-b-PDMS; (b) is high-magnification TEM image of the selected regions.

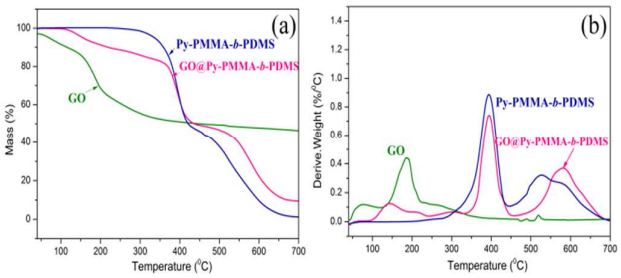

Fig.6 TGA (a) and DTG (b) curves for GO, Py-PMMA-*b*-PDMS and GO@Py-PMMA-*b*-PDMS.

Furthermore, to investigate the thermal stability of Py-PMMA-*b*-PDMS and GO@Py-PMMA-*b*-PDMS, their TGA and DTG thermograms are shown in Fig.6. GO started to lose weight upon heated below 100 °C due to the evaporation of physically adsorbed water, the main weight loss of GO took place around 200 °C (Fig.6a), presumably due to pyrolysis of the labile oxygen containing functional groups.[27] In contrast, Py-PMMA-*b*-PDMS exhibited a two-stage degradation temperature. The major loss weight loss appeared at 394 and 527 °C (Fig.6b), which should be attributed to the random main-chain scission of PMMA and PDMS segments, respectively. The decomposition temperatures were close to that of PMMA and PDMS reported in literature.[31] GO@Py-PMMA-*b*-PDMS had three major weight loss peaks (Fig. 6b) corresponding to the decomposition of GO, PMMA and PDMS segments. This further supports the successful introduction of Py-PMMA-*b*-PDMS into GO.

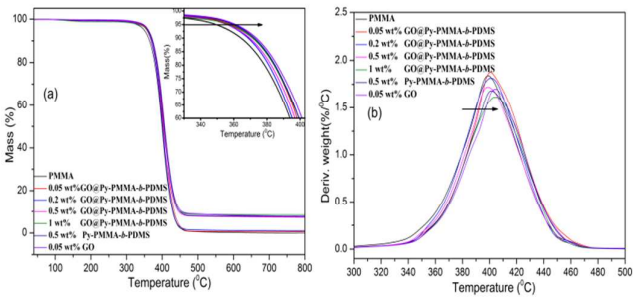

Fig.7 (a) TGA and (b) DTG curves of the pure PMMA film and composites containing different loading amounts of GO in GO@Py-PMMA-*b*-PDMS/PMMA, 0.5 wt% Py-PMMA-*b*-PDMS and 0.05 wt% GO.(inset: the TGA curve at 330-400 °C).

3.3. Properties of GO@Py-PMMA-*b*-PDMS/PMMA composites

Thermal stability The influence of GO@Py-PMMA-*b*-PDMS on the thermal stability of GO@Py-PMMA-*b*-PDMS/PMMA composite was investigated by TGA. In Fig.7, the values of $T_{d5\%}$ (the temperature of 5% weight loss) increased from 349.4 °C for PMMA to 359.5 °C for the GO@Py-PMMA-*b*-PDMS/PMMA（GO/PMMA 0.05/100）, indicating the improved thermal stability. In Fig. 7b, the maximum decomposition temperature of PMMA appeared at 398.8 °C and gradually increased with increasing GO content. For comparison, PMMA filled with 0.05 wt% GO and 0.5 wt% Py-PMMA-*b*-PDMS were separately prepared. It can be seen that both Py-PMMA-*b*-PDMS and GO could improve the thermal stability of PMMA composites, which are attributed to the barrier effect of GO and the structure of Si-O-Si.[32] In addition, the GO content in GO@Py-PMMA-*b*-PDMS was about 8.3 wt%, 27.4 wt%, 48.4 wt% and 65.8 wt%, which were carried out by XPS. So the percentage of GO in GO@Py-PMMA-*b*-PDMS/PMMA was about 0.046 wt%, 0.192 wt%, 0.484 wt% and 0.987 wt%, respectively.

From the DSC curves (Fig.S3 in the Supporting Information), the addition of 0.5 wt% Py-PMMA-*b*-PDMS into PMMA decreased the glass transition temperature (T_g) of PMMA from 116.6 to 103.6 °C. This result suggested that Py-PMMA-*b*-PDMS had a plasticizing effect owing to the flexible Si-O-Si segments. Also, the same PMMA segments in Py-PMMA-*b*-PDMS with the PMMA matrix may obtain excellent dispersing. However, PMMA composite containing 0.05 wt% GO almost had the same T_g as PMMA. Furthermore, T_g of all the composites gradually decreased with increasing GO concentration, showing a maximum decrease of 7.2 °C after addition of 1.0 wt% GO in GO@Py-PMMA-*b*-PDMS/PMMA. These results demonstrate that high loading of GO may yield more active sites to interact with Py-PMMA-*b*-PDMS by π-π stacking resulting in more uncoiled Py-PMMA-*b*-PDMS chains. Therefore, Py-PMMA-*b*-PDMS should have acted as a "bridge" between GO and PMMA matrix.

Mechanical properties Fig.8 (a) shows the typical stress-strain curves of PMMA and its composites with GO, Py-PMMA-b-PDMS and GO@Py-PMMA-b-PDMS. The Young's modulus (Fig.9b) was calculated from the slope of the linear fit in the initial section of the curve (0.5% strain). The tensile strength (Fig.8b) was the strength at failure. Compared with PMMA, composites had higher tensile strength and Young's modulus. For instance, with only addition of 0.05 wt% GO in GO@Py-PMMA-*b*-PDMS/PMMA, the tensile strength and Young's modulus of the composites sharply increased to 25.1 MPa and 1037.1 MPa (Table S2 in the Supporting Information), which increased by 53% and 22.6%, respectively. The mechanical properties of composites increased with increasing GO content, and the addition of 0.2 wt% GO in GO@Py-PMMA-*b*-PDMS/PMMA exhibited the highest stress strength and Young's modulus, increasing by 64% and 44%. However, when the content

of GO in GO@Py-PMMA-*b*-PDMS/PMMA surpassed 0.2 wt%, both the tensile strengths and Young's modulus tended to decrease, which was probably attributed to the agglomerations of GO@Py-PMMA-*b*-PDMS at high content (Fig.S4 in the Supporting Information). In comparison with composites containing 0.05 wt% GO and 0.05 wt% GO in GO@Py-PMMA-*b*-PDMS/PMMA, it was found that the latter had higher tensile strengths and Young's modulus. This reason could be that Py-PMMA-*b*-PDMS promoted GO well dispersion in matrix, resulting in obtaining more enhancement of GO. The well dispersion GO in matrix could effectively transfer the load between GO sheet and matrix.[33-35] Also the high aspect ratio of GO was effectively imparted to the composites with their rigid structure.[36] It is certain that GO@Py-PMMA-*b*-PDMS is very efficient in the enhancement of mechanical properties.

It is worth noting that the elongations at break and toughness of the composites increased with the addition of GO@Py-PMMA-*b*-PDMS (Fig.8c). At 0.05 wt% GO content in GO@Py-PMMA-*b*-PDMS/PMMA, the maximum elongation values and toughness were obtained, which increased by 117% and 218%, indicating that GO@Py-PMMA-*b*-PDMS also played a role of toughness modifier. Such a phenomenon was very different from the results of the decreased toughness accompanied by increased strength and modulus. In order to figure out the phenomenon, the composites containing 0.05 wt% GO and 0.5 wt% Py-PMMA-*b*-PDMS were prepared. As shown in Fig.8b, for only addition of 0.05 wt% GO, the tensile strengths and Young's modulus increased to 25.1 MPa and 1.0 GPa, which increased by 54% and 23%, respectively, demonstrating that the enhancement effect for composites was primarily due to the GO compared with Py-PMMA-*b*-PDMS. In terms of the Py-PMMA-*b*-PDMS, Fig.8c showed the elongation values and toughness for composites containing 0.5wt% Py-PMMA-*b*-PDMS, which dramatically increased by 124% and 112%, were much higher than composites only containing GO. The result pointed the toughening effect of composites was largely ascribed to the addition of Py-PMMA-*b*-PDMS. The flexible PDMS segments in matrix may disperse and absorb some energy to achieve the toughening effect. Therefore, in view of the mechanical properties of GO@Py-PMMA-*b*-PDMS for PMMA matrix, we have reasons to believe that GO@Py-PMMA-*b*-PDMS is an ideal reinforcing and toughening material. It can be concluded the enhancement and toughness effect for PMMA can be reached by the addition of GO@Py-PMMA-*b*-PDMS.

Moreover, many similar researches have been reported. For example, Amit Mandal et al.[22] prepared a new compatibilizer (P2) which Non-covalent interaction with CNTs and then was added into the poly(vinylidene fluoride) (PVDF) matrix. The toughness and tensile strength showed a maximum increase by 178.7% and 354.8% at ~0.3wt% CNTs content. Lian et al.[37] found that the functionalization of CNTs with Kevlar can significantly improve the mechanical properties of PMMA. At the Kevlar/CNTs content of 0.3 wt%, the tensile strengths increased by ~127%. However, the composites exhibited lower toughness effect. These increments for toughness of GO@Py-MMA-*b*-PDMS/PMMA composite films were superior to those of composites with graphene fillers reported in literature.[22, 37]

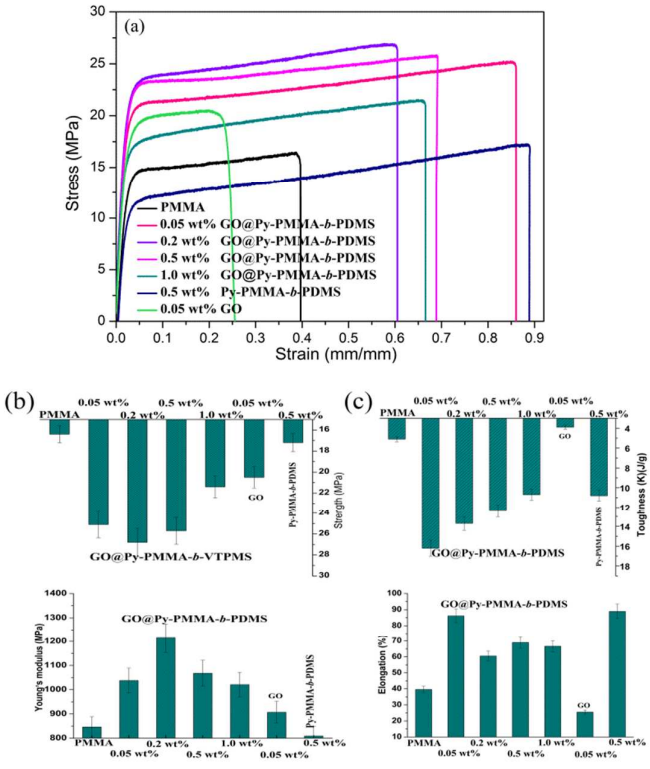

Fig. 8 (a) Typical stress-strain curves, (b) Young's modulus and tensile strengths (c) elongations and toughness values of composite films with different loading amounts of GO in GO@Py-PMMA-*b*-PDMS/PMMA, 0.5 wt% Py-PMMA-*b*-PDMS and 0.05 wt% GO.

Well known, the dispersion of fillers significantly affects the mechanical properties of composites. To check the dispersion of GO@Py-PMMA-*b*-PDMS in PMMA, SEM photos of the tensile fractured surfaces of the composites are shown in Fig.9. The tensile fracture surfaces of GO@Py-PMMA-*b*-PDMS/PMMA composites (Fig.9b-e) were more rough and rigid than PMMA (Fig.9a). With

increasing GO content, this phenomena became increasingly apparent, which implied that more energy was required to make the composites broken, leading to the improved mechanical strength.[38] Also the agglomeration of GO was not observed obviously until the content of GO reached 0.5 wt% (Fig.9d) and 1.0 wt% (Fig.9e), resulting in a slightly decreased tensile strength. To further investigate the reinforcement and toughness effects, tensile fractures of composites with addition of 0.05 wt% GO and 0.5 wt% Py-PMMA-*b*-PDMS were observed. As seen in Fig.9f, it was obvious that the GO sheets were well dispersed in PMMA, showing the well enhanced performance. While the composites containing Py-PMMA-*b*-PDMS exhibited more "stripes" and "hollow" in the tensile fracture surfaces, indicating phase separation might occur in composite (PDMS dispersed phase and PMMA continuous phase). This structure can play excellent toughening effect, indicating that Py-PMMA-*b*-PDMS was primarily contributed to toughening effect of composites.

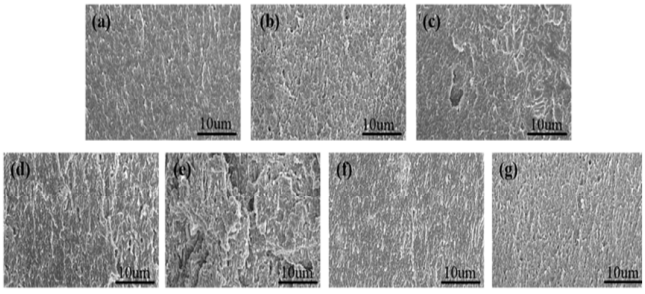

Fig. 9 SEM fractographs of the (a) pure PMMA film, GO@Py-PMMA-*b*-PDMS/PMMA composite with different loading amounts of GO in GO@Py-PMMA-*b*-PDMS/PMMA: (b) 0.05 wt%, (c) 0.2 wt%,(d) 0.5 wt%,(e) 1.0 wt%, (f) 0.05 wt% GO and (g) 0.5 wt% Py-PMMA-*b*-PDMS.

Optical properties Fig.10a presents images of PMMA and composite films with GO, Py-PMMA-*b*-PDMS and GO@Py-PMMA-*b*-PDMS. With increase GO content in GO@Py-PMMA-*b*-PDMS, the light transmittance of composite films was gradually reduced. Specifically, when the GO@Py-PMMA-*b*-PDMS content surpassed 0.5 wt%, the light transmittance of the composite films was completely opaque (Fig.10b). In order to compare the effects of GO and Py-PMMA-*b*-PDMS on composite transmittance, composite films containing 0.05 wt% GO and 0.5 wt% Py-PMMA-b-PDMS maintained a high transparency. However, the light transmittance of Py-PMMA-*b*-PDMS/PMMA composite film is higher than GO/PMMA, indicating that GO has a greater impact on the composites transparency. Under 400nm, the transmittance of these composite films decreased conspicuously. These films may scatter and absorb ultraviolet light, indicating that they have UV-shielding function. Moreover, GO/PMMA and GO@Py-PMMA-*b*-PDMS/PMMA composite films possessed high refractive index and haze. Composite film containing 0.05 wt% GO in GO@Py-PMMA-*b*-PDMS showed 16.8% haze, which was much higher than PMMA (2.1%). As also shown in Fig.11, it can be observed that the refractive index of Py-PMMA-*b*-PDMS/PMMA and GO@Py-PMMA-*b*-PDMS/PMMA varied from 1.480 to 1.511, showing a good linear relationship between the polymer refractive index and GO content. The refractive index can be predicted through Lorentz - Lorenz eqn (1)[39], which expresses the correlation among the refractive index (n), the molecular refraction (R), molecular weight (M), and molecular volume (V) of the polymer repeating unit.

$$\frac{n^2-1}{n^2+2}=\frac{R}{M}\rho=\frac{R}{M}\frac{M}{V}=\frac{R_M}{V_M} \quad (1)$$

The eqn (1) is transformed into eqn (2)

$$n=\sqrt{\frac{1+2(R_M/V_M)}{1-(R_M/V_M)}} \quad (2)$$

where R/M can be further termed as molar refraction (R_M), M/V can be defined as the reciprocal of molar volume (V_M). According to Eqn (2), the refractive index of the materials was directly proportional to the electronic polarizability and density. In general, strategies to improve the refractive index of the composite typically comprised introducing some functional groups with larger molar refraction (R_M) and metal element or metallic oxides. Moreover, graphene possesses a high refractive index (n=2.6–3) and low density.[40-41] Therefore, GO is also beneficial for increasing the refractive indices of polymers. The optical properties of polymers like PMMA are very important, especially for applications in flexible displays, e-paper, organic light-emitting diodes (OLEDs) and organic photovoltaics (OPVs). Therefore, the optical property broadened the application of GO@Py-PMMA-*b*-PDMS.

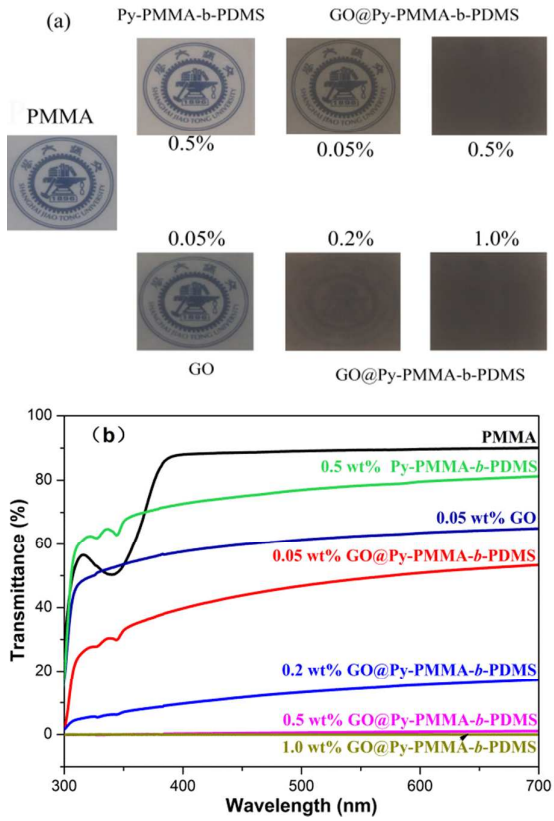

Fig. 10 The effect of GO, Py-PMMA-*b*-PDMS and GO@Py-PMMA-*b*-PDMS on the optical transparency and UV-vis transmittance of the composite films: (a) photographs showing the transparency of samples; (b) Optical transmission spectra of composite films.

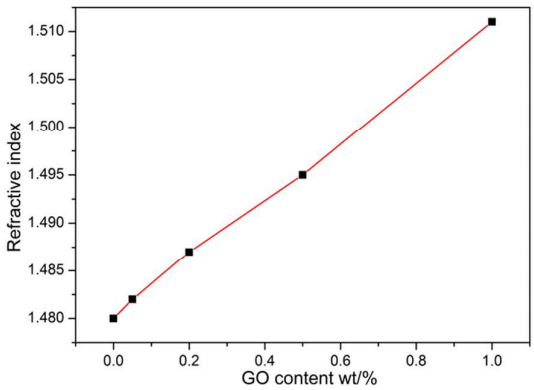

Fig. 11 Dependence of refractive index of GO@Py-PMMA-*b*-PDMS/PMMA composites on the GO content

4. Conclusion

Pyrene moiety modified block copolymer Py-PMMA-*b*-PDMS was synthesized by an ARGET-ATRP method. Its functionalization efficiency to GO through non-covalent interaction (π-π stacking) between the pyrene group and the graphitic surface of GO was characterized by TGA, XPS, UV-Vis, PL and TEM techniques. The resultant GO@Py-PMMA-*b*-PDMS particles were further dispersed into PMMA via a solution blending method. It is found that the GO@Py-PMMA-*b*-PDMS particles could be well dispersed in PMMA at the concentration varying from 0.05 to 1.0 wt%. The Young's modulus and tensile strength of the composites reached their maximum values of 1.21 GPa and 26.8 MPa, respectively, with the addition of 0.2 wt% GO. With the addition of 0.05 wt% of GO@Py-PMMA-*b*-PDMS, the elongation at break and tensile toughness of PMMA dramatically increased by 117% and 218%, respectively, indicating the GO@Py-PMMA-*b*-PDMS could reinforce and toughen PMMA simultaneously at lower concentration. In addition, the optical properties and thermal stability of PMMA were enhanced by the addition of GO@Py-PMMA-*b*-PDMS, indicating such non-covalent bonded GO@Py-PMMA-*b*-PDMS is an ideal filler for fabrication of high-performance PMMA nanocomposites with balanced mechanical, optical and thermal properties.

Acknowledgements

The authors acknowledge the financial support from National Natural Science Foundation of China (No. 51273109，51235008) and the discussion with Ms. Lin Qiu from Blue Star Company, China.

References

1 M. Hirata, T. Gotou, S. Horiuchi, M. Fujiwara and M. Ohba, *Carbon*, 2004, 42, 2929-2937.

2 H. Kim, A. A. Abdala and W. Macosko, *Macromolecules*, 2010, 43, 6515-6530.

3 N. R. Wilson, P. A. Pandey, R. Beanland, R. J. Young, I. A. Kinloch, L. Gong, Z. Liu, K. Suenaga, J. P. Rourke, S. J. York and J. Sloan, *ACS Nano*, 2009, 3, 2547-2556.

4 C. Bao, Y. Guo , L. Song , Y. Kan, X. Qian and Y. Hu, *J. Mater. Chem., 2011, 21, 13290-13298.*

5 H. Kim, Y. Miura and C.W. Macosko, *Chem. Mater.*, 2010, 22, 3441–3450.

6 J. R. Potts, D. R. Dreyer, C. W. Bielawski and R.S. Ryoff, *Polymer,* 2011, 52, 5-25.

7 Y. Li, R. Umer, Y. A. Samad, L. Zheng, K. Liao, *Carbon*, 2013, 55, 321-327.

8 Xi.G. Mei, J.Y. Ouyang, *Carbon*, 2011, 49, 5389-5397.

9 G.Q. Qi, J. Cao, R. Y. Bao, Z. Y. Liu, W. Yang, B. H. Xie and M. B. Yang, *J. Mater. Chem. A,* 2013, 1, 3163–3170.

10 K. R. Paton, E. Varrla, C. Backes, et al., *Nature materials,* 2014, 13, 624-630.

11 H. X. Tang, G. J. Ehlert, Y. R. Lin and H. A. Sodano, *Nano letters,* 2011, 12, 84-90.

12 S. Wang, P. J. Chia, L. L. Chua, L. H. Zhao, R. Q. Png, S. Sivaramakrishnan, M. Zhou, R. G. S. Goh, R. H. Friend, A. T. S. Wee and P. K. H. Ho, *Adv. Mater.,* 2008, 20, 3440-3446.

13 Z. Liu, J.T. Robinson, X. Sun and H. Dai, *J. Am. Chem. Soc.,* 2008, 130, 10876-10877.

14 E. Bekyarova, M. E. Itkis, P. Ramesh, C. Berger, M. Sprinkle, W. A. de Heer and R. C. Haddon, *J. Am. Chem. Soc.,* 2009, 131, 1336-1337.

15 Y. X. Xu, H. Bai, G. W. Lu, C. Li and G. Q. Shi, *J. Am. Chem. Soc.,* 2008, 130, 5856-5857.

16 R. Hao, W. Qian, L. Zhang and Y. Hou, *Chem. Commun.,* 2008, 48, 6576-6578.

17 X. Zhang, M.Zhu, P.Chen, Y.Li, H.Liu, Y.Li and M.Liu, *Phys. Chem. Chem. Phys.*, 2015, 17, 1217-1225.

18 Y. Xu, Q. Wu, Y. Sun, H. Bai and G. Shi, *ACS Nano,* 2010, 4, 7358-7362.

19 Y. Wang, X. Chen, Y. Zhong, F. Zhu and K. P. Loh, *Appl. Phys. Lett.,* 2009,95, 063302.

20 H. Bai, Y. Xu, L. Zhao, C. Li and G. Shi, *Chem. Commun.,* 2009, 13, 1667-1669.

21 H. Wu, W. Zhao, H. Hu and G. Chen, *J. Mater. Chem.,* 2011, 21, 8626-8632.

22 M. Amit, and A. K. Nandi, *J. Phys. Chem. C*, 2012, 116, 9360-9371.

23 X. Bai, C.Y. Wan, Y. Zhang and Y.H. Zhai, *Carbon, 2011, 45, 1608-1613.*

24 J. Babin, M. Lepage and Y. Zhao, *Macromolecules,* 2008, 41, 1246-1253.

25 L. Bai, Li. Zhang, Z. Zhang, J. Zhu, N. Zhou, Z. Cheng and X. Zhu, *J. Polym. Sci., Part A: Polym. Chem.,* 2011, 49, 3970-3979.

26 J. Fan, Z. Shi, M. Tian, J. Wang and J. Yin, *ACS Appl. Mater. Interfaces,* 2012, 4, 5956-5965.

27 S. H. Lee, D. R. Dreyer, J. An, A. Velamakanni, R. D. Piner, S. Park, Y. Zhu, S.O. Kim, C.W. Bielawski and R. S. Ruoff, *Macromol. Rapid Commun.,* 2010, 31, 281–288.

28 Q. Bao, H. Zhang, J. Yang, S. Wang, D. Y. Tang, R. Jose, S. Ramakrishna, C. T. Lim, and K. P. Loh, *Adv. Funct. Mater,* 2010, 20, 782–791.

29 H. J. Kim, J. Sung, H. Chung, Y. J. Choi, D. Y. Kim, and D. Kim, *J. Phys. Chem. C*, 2015, 119 , 11327–11336.

30 J. Chen, H. Liu, W. A. Weimer, M. D. Halls, D. H. Waldeck and G. C. Walker, *J. Am. Chem. Soc.,* 2002, 124, 9034-9035.

31 J. Liang, L. He, X. Zhao, X. Dong, H. Luo and W. Li, *J. Mater. Chem.,* 2011, 21, 6934–6943.

32 T. C. Chang, Y. C. Chen, S. Y. Ho and Y. S. Chiu, *Polymer*, 1996, 37, 2963-2968.

33 G. Goncalves, P. A. A. P. Marques, A. B. Timmons, B .Bdkin, M. K. Singh, N. Emamic and J. Gracioa, *J. Mater. Chem.,* 2010, 20, 9927–9934.

34 K. K. Sadasivuni, A. Kafy, L. Zhai, H. U. Ko, S. Mun and J. Kim, *Small,* 2015, 11, 994-1002.

35 N. Yousefi, X. Sun, X. Lin, X. Shen, J. Jia, B. Zhang, and J. K. Kim, *Adv. Mater.,* 2014, 26, 5480-5487.

36 S. Morimune, T. Nishino and T. Goto, *ACS Appl. Mater. Interfaces,* 2012, 4, 3596−3601.

37 M. Lian, J. C. Fan, Z. X. Shi, H. Li, J. Yin, *Polymer,* 2014, 55 2578-2587.

38 Y. Wang, Z. Shi, J. Yin, *J. Phys. Chem. C,* 2010, 114, 19621–19628.

39 J. C. Seferis, in Polymer Handbook, ed. J. Brandrup and E. H. Immergut, Wiley, New York, 3rd edn, 1989.

40 Z. H. Ni, H. M. Wang, J. Kasim, H. M. Fan, T. Yu, Y. H. Wu,Y. P. Feng and Z. X. Shen, *Nano Lett.,* 2007, 7, 2758-2763.

41 A. K. Geim and K. M. Novoselov, *Nat. Mater.,* 2007, 6, 183-191.